Nat Hazards (2014) 71:1475–1493
DOI 10.1007/s11069-013-0957-7

ORIGINAL PAPER

Measurement of pressure drop in drainage boreholes and its effects on the performance of coal seam gas extraction: a case study in the Jiulishan Mine with strong coal and gas outburst dangers

Qingquan Liu · Yuanping Cheng

Received: 16 October 2013 / Accepted: 13 November 2013 / Published online: 23 November 2013

Abstract Although it is a well-accepted belief in the petroleum industry that horizontal well productivity can be limited by the pressure drop within the wellbore, little has been reported regarding how this pressure drop affects gas extraction from a coal seam and its further effects on mitigating coal and gas outburst dangers in coal. One of the major reasons for this scarcity is that the pressure-drop distribution in horizontal drainage boreholes is difficult to obtain. In this study, measurements of pressure drops in 54 drainage boreholes were performed in the No. 2_1 coal seam, which is the primary mining layer of Jiulishan Mine and poses a strong danger of coal and gas outbursts. Next, a coupled governing finite-element model, which includes the pressure drop in the borehole, Darcy flow in fractures, gas diffusion in the matrix blocks, and the dynamic evolution of the permeability of coal, was developed and implemented using a finite-element method to quantify the pressure-drop effects. Field tests of the pressure drops indicate that the pressure increases in a parabolic form with the increasing depth of the borehole, and lower outer end pressure is associated with larger pressure increments. The numerical results indicate that the pressure drop does affect the coal seam gas extraction, the pressure around the borehole increases with increasing borehole depth, and the increment of the pressure becomes larger when the borehole's drainage effect is enhanced. However, the impact is small and can be ignored in engineering.

Keywords Coal and gas outburst disaster · Horizontal drainage borehole · Pressure drop · Gas–coal interactions

Q. Liu · Y. Cheng (✉)
Faculty of Safety Engineering, China University of Mining and Technology, Xuzhou 221116, China
e-mail: cumtsafe@gmail.com

Q. Liu · Y. Cheng
National Engineering Research Center for Coal and Gas Control, Faculty of Safety Engineering, China University of Mining and Technology, Xuzhou 221116, China

Y. Cheng
State Key Laboratory of Coal Resources and Safe Mining, China University of Mining and Technology, Xuzhou 221008, China

1 Introduction

The No. 2_1 coal seam is the primary mining layer of Jiulishan Mine and is characterized by strong coal and gas outburst danger. More than 60 sudden coal and gas outbursts have occurred during coal mining since 1980. The No. 2_1 coal seam is also characterized by high gas pressure and gas content. Data from the present mining zone are as follows: The gas pressure ranges from 0.86 to 2.08 MPa, the gas content ranges from 8 to 33 m^3/t, and the gas pressure and content both have a tendency to rise with the increase in mining depth. In addition, methane has the second greatest radiative forcing among the long-lived greenhouse gases; it accounts for 14.3 % of the global anthropogenic greenhouse gas emissions (Olivier et al. 2005), and its greenhouse effect is approximately 21 times that of CO_2 (SHEN et al. 2007). If the methane were emitted freely, it would enter the atmosphere and cause serious environmental harm. Degassing coal seams with horizontal gas drainage boreholes is the most important engineering method for mitigating these hazards in the Jiulishan Mine and results in the beneficial recovery of a clean-burning, low-carbon fuel resource. The success of degassing coal seams depends on our understanding of gas migration around drainage boreholes and their interactions.

The mechanism of methane gas migration around drainage boreholes is based on the coupling of flow in the coal seam and in drainage boreholes. The gas–coal interactions have been studied by many researchers (Valliappan and Zhang 1996; Zhu et al. 2007; Zhang et al. 2008; Hu et al. 2009). However, little has been known of how this pressure drop affects the coal seam gas extraction and its further effects on mitigating the danger of coal and gas outbursts. Due to the pressure drop, the front end of the drainage borehole has a higher production pressure drawdown than does the rear end, and this difference may well affect the performance of the drainage boreholes. That horizontal well productivity can be limited by the pressure drop within the wellbore is a well-accepted belief in the petroleum industry (Su and Gudmundsson 1998). It is thus necessary to study the effects of pressure drop on the performance of coal seam drainage boreholes.

In 1990, Dikken (1990) presented a theoretical model for understanding and predicting the influence of wellbore inflow on the pressure drop, and since then, much theoretical and experimental study on the pressure drop in horizontal wells has been conducted by many researchers (Su and Gudmundsson 1998; Firoozabadi et al. 2011; Ouyang and Aziz 2000; Badie et al. 2000; Li et al. 2007; Sarica et al. 1994; Awwad et al. 1995; Dikken 1990; Novy 1995; Amna and Hiroshi 2011; Yuan et al. 1996; Guo 2010). However, the roughness of the drainage borehole in a coal seam is greater than that of the horizontal well. Moreover, being limited by the low strength of the coal seam, the stability of the drainage borehole in the coal seam is poorer than that of the horizontal wells that are widely used in the petroleum industry (Qu et al. 2011). In particular where it penetrates weak structural zones, the drainage borehole may be easily damaged (Yao et al. 2010), coal fragments falling from the borehole wall may partially block the borehole, and the smallest particles may move with the gas flow. These factors may have a great impact on the overall distribution of the pressure drop and are not included in conventional pressure-drop models. As a result, these conventional models may not be useful for correct predictions of the pressure-drop distribution of drainage boreholes in coal seams.

The primary aim of this study was to measure the pressures inside the methane drainage boreholes in the Jiulishan Mine and obtain their pressure-drop distributions. Next, a coupled governing finite-element model, which includes the pressure drop in the borehole, Darcy flow in fractures, gas diffusion in the matrix blocks, and the dynamic evolution of permeability of coal seam, was developed and implemented using a finite-element method to quantify these

pressure-drop effects. The residual gas pressure and relative gas content in the coal seam was used as the evaluation indexes. Finally, the study findings provided theoretical support for rational gas extraction to mitigate the potential for future gas disasters in the Jiulishan Mine.

2 Background of the study area

The Jiaozuo Coalfield is located in northern Henan Province in China. The Jiulishan Mine is located in the central part of the Jiaozuo Coalfield and spans an area of 18.6 km^2. The No. 2_1 coal seam is the primary mined layer in the Jiulishan Mine and is characterized by a high danger of coal and gas outbursts. More than 60 sudden coal and gas outbursts have occurred during coal mining since 1980, and the locations of these outbursts are distributed throughout the coal mine (Fig. 1). The most intense coal and gas outburst occurred in the 15,051 roadway of the Jiulishan Mine (August 23, 2005), with 2,397 tons of coal and 230,000 cubic meters of methane gas bursting forth. The latest outburst occurred in the 16031 driving working face, claiming 18 lives (October 27, 2011).

The No. 2_1 coal seam is also characterized by high gas pressure and gas content. Data from the present mining zone are as follows: The gas pressure ranges from 0.86 to 2.08 MPa, and the gas content ranges from 8 to 33 m^3/t. Both of these parameters have a tendency to rise with the increase in mining depth (Figs. 2, 3). The coal and gas outburst danger in the No. 2_1 coal seam increases in a similar fashion. Degassing the coal seams with horizontal gas drainage boreholes is the most important engineering method to mitigate the outburst danger in the Jiulishan Mine. It was thus necessary to study how the pressure drop in horizontal gas drainage boreholes affects the coal seam gas extraction and its further effects on mitigating the danger of coal and gas outbursts in the coal seam. Such

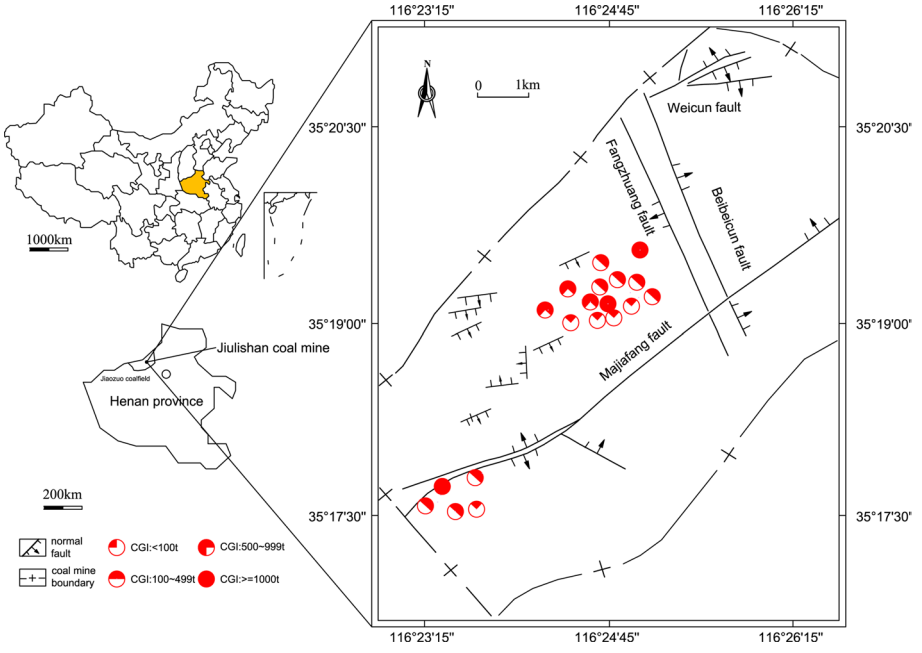

Fig. 1 Map showing the study area and locations for coal and gas outbursts (CGI denotes the intensity of coal and gas outburst)

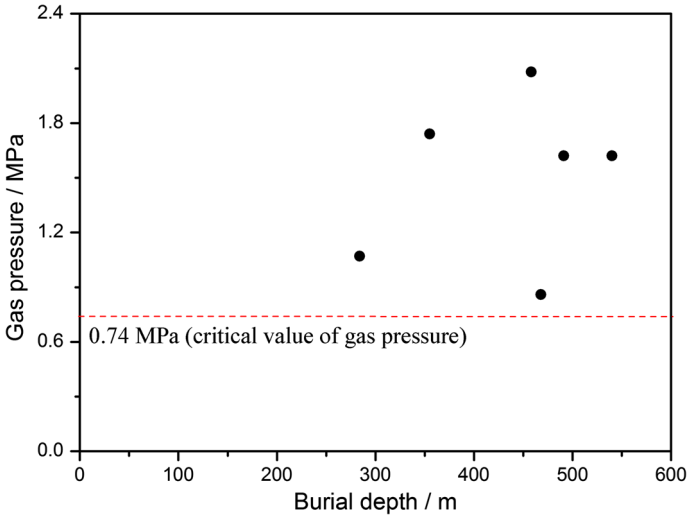

Fig. 2 Relationships between gas pressure and burial depth in Jiulishan Mine

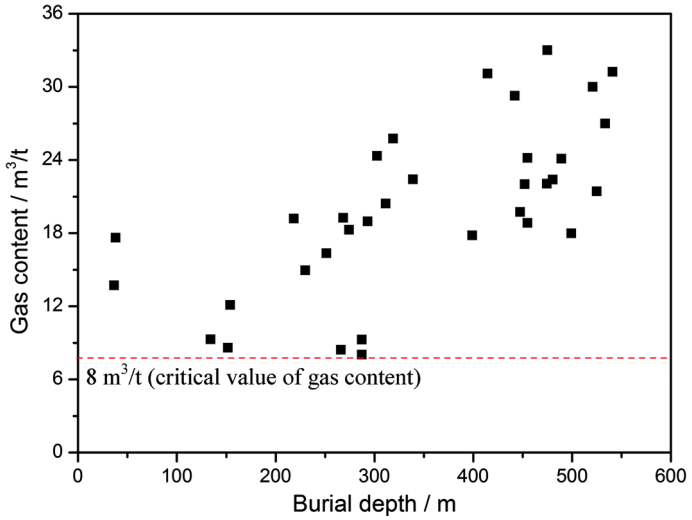

Fig. 3 Relationships between gas content and burial depth in Jiulishan Mine

research findings may contribute to a program of gas extraction to mitigate the potential for future gas disasters in the Jiulishan Mine.

3 Research into the pressure drop

3.1 A brief review of pressure-drop calculations in horizontal wells

As shown in Fig. 4, during the production stage of the horizontal well, and due to the wall friction of the horizontal well, a pressure drop occurs as the fluid flows from the rear to the

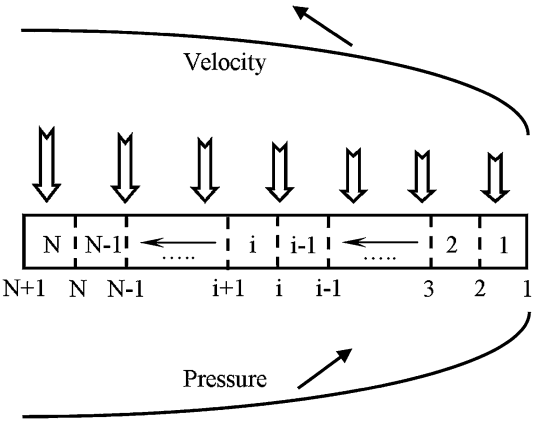

Fig. 4 Schematic of variable mass flow in the horizontal borehole

front of the horizontal well. Unlike the conventional pipe flow, fluid will continually enter the well through the wall. This flow is a type of variable mass flow with an increase in the fluid quality along the flow direction (Yu et al. 2001). The increasing flow velocity, and therefore momentum, contributes to the pressure drop (Su and Gudmundsson 1998). Moreover, the mixing between wellbore flow and perforation flow and the effect of gravity also contribute to the pressure drop.

Three of the pressure-drop models that are more common in industry are those of Su and Gudmundsson (1998), Yuan et al. (1996), and Ouyang and Aziz (2000). According to the model of Z. Su, the total pressure drop in a horizontal wellbore consists of four pressure-drop terms.

$$\Delta p = \Delta p_{\text{wall}} + \Delta p_{\text{acc}} + \Delta p_{\text{perf}} + \Delta p_{\text{mix}} \tag{1}$$

where Δp is the total pressure drop, Pa; Δp_{wall} is the wall frictional pressure drop, Pa; and Δp_{acc} is the acceleration pressure drop, Pa. The last two pressure-drop terms, Δp_{perf} and Δp_{mix}, Pa, are due to perforation roughness and mixing effects, respectively, which need to be determined experimentally. For a horizontal well divided into N equal segments, the pressure drop due to pipe wall friction, Δp_{wall}, can be represented as

$$\Delta p_{\text{wall}} = \sum_{i=1}^{N} \left(f \frac{\Delta L_i}{D} \frac{\rho u_i^2}{2} \right) \tag{2}$$

The pressure drop due to momentum change, Δp_{acc}, can be represented as

$$\Delta p_{\text{acc}} = \sum_{n=1}^{N} \rho \left(u_{n+1}^2 - u_n^2 \right) \tag{3}$$

where u represents the mean flow velocity, m/s; f is the friction factor of the well; and ρ is the fluid density, kg/m^3. The subscripts "i" and "n" donate the ith segment and the nth section of the well, respectively (Fig. 4). The previous section is just a brief summary of the Z. Su model; additional details are presented by Su and Gudmundsson (1998).

Although the Z. Su model serves well in predicting the pressure drop in horizontal wells in the oil industry, it faces the following problems when predicting the pressure drop in boreholes in a coal seam:

1. Due to the large compressibility of the gas, the density of the gas along the borehole cannot stay constant, whereas in the Z. Su model, this value is usually set as a constant.

2. The roughness and nonuniformity of the borehole wall in a coal seam are both greater than those of a horizontal well wall.
3. Limited by the low strength of the coal, the stability of the drainage borehole in the coal seam is poorer than that of the horizontal wells widely used in the petroleum industry (Qu et al. 2011). In particular where it penetrates weak structural zones, the drainage borehole may be easily damaged (Yao et al. 2010), the coal fragments falling from the borehole wall may partially block the borehole, and the small particles may move with the gas flow. These factors may have a considerable impact on the overall distribution of pressure drop and are not included in conventional pressure-drop models.

The conventional pressure-drop models thus may not be useful for correct predictions of the pressure-drop distribution of a drainage borehole in a coal seam.

3.2 Measurements of pressure drop in Jiulishan Mine

Eighteen sets of field tests were performed to develop an understanding of the pressure-drop distribution along a drainage borehole in a coal seam. In China, such as in the Jiulishan Mine, the length of the borehole is usually half the width of the working face, i.e., approximately 90–100 m. It was helpful for us to perform the field tests under these conditions.

The experiment site was located in the 16031 return airway in the 16th mining area of the Jiulishan Mine. The 16031 return airway is approximately 400 m long. The No. 2_1 coal seam has an average thickness of 3.5 m in the area of the 16031 return airway, and the dip angle of the No. 2_1 coal seam is approximately 12.2°. The test area had not yet been degassed, except for the area near the roadway, and was not mined during the experiments, thus providing a safe and reliable experimental site. The test borehole's dip angle, diameter, and length were 12°, 94 mm, and 100 m, respectively (Fig. 5). The latter two parameters match those of the drainage boreholes widely used in the Jiulishan Mine. Copper tubes with an inside diameter of 12.7 mm were used as the piezometric tube, and U-Hg meters were used to test the pressures. Due to the limited test borehole diameter, we were unable to place a sufficient number of copper tubes to test the pressures at different depth in a single borehole. A compromise scheme was proposed: Several groups of boreholes would be tested, each consisting of three testing boreholes with the same specifications. The spacing between adjacent boreholes within a group was 3 m, whereas the spacing between adjacent groups was 8 m. Above all, the pressure at the outlets of the boreholes was kept equal during the experiment.

The copper tubes and a PVC extraction tube were inserted into the completed borehole. The copper tubes extended approximately 30 mm out of the boreholes. The lengths of the various tubes differed by 10 m to obtain the pressures at depths of 30–90 m inside the boreholes. All of the copper tubes were marked at the outer ends and tied together with iron wire. Thus, in each group, two boreholes were used to obtain the pressures at two different depths, while the third borehole was used to obtain the pressures at three different depths. The boreholes were sealed using polyurethane material, and the sealed length was approximately 15 m. Yellow mud was used to seal the outer end of the borehole to obtain better sealing performance. The inside diameter of the PVC extraction tube was 25.4 mm. The PVC extraction tube was connected to an extraction line system with an inside diameter of 25.4 mm. The sample size was large to reduce unpredictable errors. The pressures from 54 test boreholes were obtained in this study.

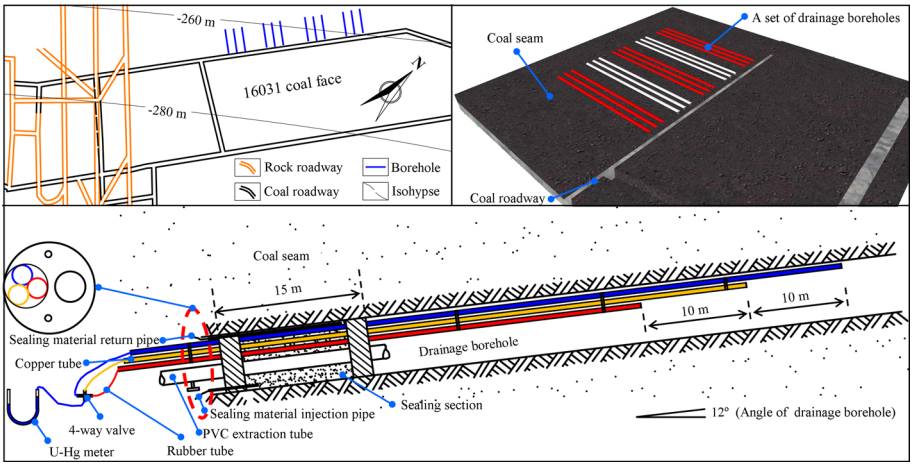

Fig. 5 Schematic of the test site and arrangement of the testing borehole

The U-Hg meter was connected to the copper tubes using rubber tubes and a three-way valve (or a 4-way valve). When starting the tests, first the valve between the PVC extraction tube and the extraction line system was opened, and then the outlet pressure of the borehole in a group at a same level was maintained. The copper tubes were tested in succession, meaning that when one was being tested, the others were closed. When the liquid level in the U-Hg meter remained stable for 30 min, we were able to obtain credible experimental data. The experimental data were converted into pressures, which are listed in Table 1.

The pressures ranged from 58.7 to 76.1 kPa near the outer ends of the boreholes and from 66.4 to 80.4 kPa at a depth of 90 m inside the boreholes. For further analysis, four sets of data were selected from Table 1 and are plotted in Fig. 6. The pressures near the outer ends of the boreholes were the basis for the selection to ensure that the maximum, minimum, and intermediate values were all included.

Figure 6 illustrates the pressure distributions in the No. 1, No. 7, No. 12, and No. 18 boreholes. As mentioned above, a PVC extraction tube passed through the sealed section of the borehole and connected the borehole with the extraction line system. The PVC extraction tube was approximately 15 m long, and the roughness of its inner wall was far less than that of the borehole wall; in other words, the pressure drop along the PVC extraction tube was small. For the sake of data analysis, the small pressure drop in the PVC extraction tube was ignored. Therefore, each set of data begins at $x = 15$ m, as shown in Fig. 6. It is clear that the pressure increases in a parabolic form with the increase in the borehole depth. The maximum and minimum pressure gradients were observed in the No. 18 and No. 1 boreholes, respectively. The pressure gradients in the No. 7 and No. 12 borehole were of intermediate values. The lower the outer end pressure, the larger the pressure gradient between coal seam and a drainage borehole. Then more gas will be extracted into the drainage borehole. The increase in the gas mass will lead to the increase in gas pressure drop in a drainage borehole (Dikken 1990; Yuan et al. 1996; Ouyang and Aziz 2000). Therefore, the lower the outer end pressure, the larger the pressure gradient in a borehole. The fitting function used to calculate the pressures at various positions in a borehole is

$$p(l) = k_1 l^2 + k_2 l + p(l_{15}) \quad (15 \le l \le 90) \tag{4}$$

Table 1 Gas pressure distribution along testing boreholes

Borehole	Pressures at different depths of a borehole/kPa							
	0/m	30/m	40/m	50/m	60/m	70/m	80/m	90/m
1	76.1	76.3	76.6	76.9	77.4	78.5	79.9	80.4
2	75.8	76.1	76.1	76.6	77.3	78.2	79.2	80.1
3	72.5	72.8	73.3	73.6	74.5	75.5	76.6	77.9
4	70.9	71.0	71.1	71.2	72.5	73.6	75.3	77.3
5	70.9	71.1	71.2	71.3	72.8	73.6	75.5	77.3
6	70.9	71.1	71.2	71.6	72.9	73.6	75.5	77.4
7	70.1	70.3	70.8	71.4	72.2	73.0	75.9	77.0
8	69.8	69.9	70.1	70.4	71.2	72.5	75.8	76.1
9	69.8	69.9	70.2	70.8	71.8	73.2	75.9	77.1
10	69.5	69.7	69.9	70.1	71.6	72.8	74.7	76.7
11	69.5	69.7	69.9	70.1	71.2	72.4	74.6	76.6
12	69.3	69.5	69.8	70.8	71.3	72.5	74.2	76.2
13	69.3	69.6	69.9	70.4	71.4	72.5	74.4	76.5
14	69.3	69.7	70.1	70.7	71.3	72.5	75	76.2
15	68.7	69.1	69.6	70.2	70.9	72.1	73.6	75.7
16	68.7	69.1	69.3	69.9	70.8	72	73.5	75.6
17	59.2	59.5	59.9	60.7	61.6	63.4	64.8	67
18	58.7	59.1	59.6	60.1	60.8	62.7	64.5	66.4

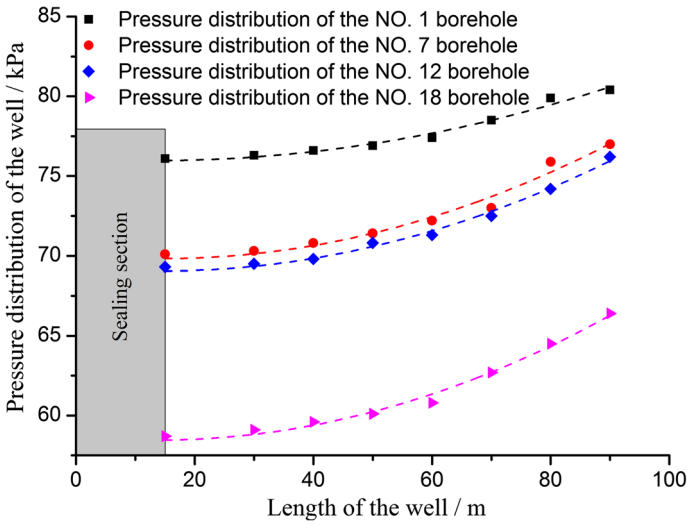

Fig. 6 Relationships between gas pressure and length of the drainage borehole

where l is the depth of the borehole, which ranges from 15 to 90, m; $p(l)$ is the pressure at the l-m depth in the borehole, kPa; $p(l_{15})$ is the experiment result and denotes the pressure on the outer end of the borehole, kPa; and k_1 and k_2 are both fitting parameters. The above four experimental results were used in Eq. 4 to calculate the fitting parameters, and the

Table 2 Fitting results and fitting precisions

Borehole	k_1	k_2	$p(l_{15})$/kPa	$p(15)$/kPa	R-squared
1	7.79E−4	−0.02025	76.1	75.97	0.9782
7	1.27E−3	−0.03718	70.1	69.83	0.9719
12	1.21E−3	−0.03474	69.3	69.05	0.9903
18	1.34E−3	−0.03614	58.7	58.46	0.9886

$p(l_{15})$ is the experiment result and denotes the pressure at the depth of 15 m in the borehole

$p(15)$ is calculated by the Eq. 4, and it denotes the pressure at the depth of 15 m in the borehole

results are listed in Table 2. The four fitting functions obtained are plotted in Fig. 6. The R-squared coefficient was used to verify the accuracy of the fitting function. The larger the value of R-squared, the more accurate the fitting function (Jin et al. 2001; Gong and Tian 2013). Table 2 shows that the values of R-squared are greater than 0.97, and thus, the fitting functions provide good fitting precision.

4 Governing equations

The mathematical model is based on the following simplifying assumptions:

1. The coal seam is dry, and methane is the only moving substance in it (water and other gases are neglected);
2. The system is isothermal;
3. Methane behaves as an ideal gas, and its viscosity is constant under isothermal conditions;
4. The CBM reservoir is a homogeneous, isotropic, and dual poroelastic medium;
5. Coal is saturated by gas.

4.1 Deformation of porous medium

For the coal seams, the effective stress laws for multiporosity media need to be taken into account (Zhang et al. 2004; Mian and Zhida 1999)

$$\sigma_{ij}^{e} = \sigma_{ij} - (\beta_f p_f + \beta_m p_m)\delta_{ij} \tag{5}$$

where σ_{ij}^{e} is the effective stress. σ_{ij} is the total stress (positive in tension). δ_{ij} is the Kronecker delta tensor. p_f is the pressure in fractures, MPa. p_m is the pressure in coal matrix blocks, MPa. β_f and β_m are effective stress coefficients for the fractures and matrix, respectively, and can be expressed as(Mian and Zhida 1999)

$$\beta_f = 1 - \frac{K}{K_m} \tag{6}$$

$$\beta_m = \frac{K}{K_m} - \frac{K}{K_s} \tag{7}$$

where K is the bulk modulus of coal, MPa, where $K = E/3(1-2\upsilon)$. K_m is the bulk modulus of the coal grains, MPa, where $K_m = E_m/3(1-2\upsilon)$. K_s is the bulk modulus of the coal skeleton, MPa. K_s usually cannot be directly measured; however, it can be calculated

using the equation (Pabst et al. 2006) $K_s{=}K_m/\{1-3\phi_m(1-\upsilon)/[2(1-2\upsilon)]\}$. E is the Young's modulus of the coal, MPa. E_m is the Young's modulus of the coal grains, MPa. υ is the Poisson's ratio of the coal.

The equations of equilibrium and the strain–displacement relationship can be expressed, respectively, as

$$\sigma_{ij,j} + F_i = 0 \tag{8}$$

and

$$\varepsilon_{ij} = \frac{1}{2}(u_{i,j} + u_{j,i}) \tag{9}$$

where F_i denotes the component of the body force in the i-direction. ε_{ij} denotes the component of the total strain tensor. u_i denotes the component of the displacement in the i-direction.

The constitutive relations for the coal seam can be expressed as

$$\sigma_{ij} = 2G\varepsilon_{ij} + \frac{2G\upsilon}{1-2\upsilon}\varepsilon_v\delta_{ij} - \beta_f p_f \delta_{ij} - \beta_m p_m \delta_{ij} \tag{10}$$

where G is the shear modulus of coal, MPa. $\varepsilon_v = \varepsilon_{11} + \varepsilon_{22} + \varepsilon_{33}$ is the volumetric strain of coal matrix.

Combining Eqs. (8), (9), and (10) yields the Navier equation as

$$Gu_{i,jj} + \frac{G}{1-2\upsilon}u_{j,ji} - \beta_f p_{f,i} - \beta_m p_{m,i} + F_i = 0 \tag{11}$$

4.2 Gas flow equation

The transfer of free methane gas through the fractures in the coal seam is governed by a mass conservation equation:

$$\frac{\partial m_f}{\partial t} + \nabla(\rho_g \vec{V}) = Q_s(1-\phi_f) \tag{12}$$

where ρ_g is the gas density at the in situ condition, kg/m^3. $\vec{V}$ is the gas velocity in fractures, m/s. Q_s is the gas exchange rate per volume of coal matrix blocks, kg/(m^3 s). ϕ_f is the fracture porosity, %. The gas mass content m_f contains only free gas in the fractures, and it can be expressed by

$$m_f = \rho_g \phi_f \tag{13}$$

By applying the ideal gas law, the relationship between gas density and pressure can be described as

$$\rho_g = \frac{M}{RT}p_f \tag{14}$$

where M is the molar mass of methane, kg/mol. R is the universal gas constant, J/(mol K). T is the temperature, K. p_f is the gas pressure in the fractures, MPa.

Volumetric flow in the fractures is governed by Darcy's law, modified to account for the Klinkenberg effect (Gilman and Beckie 2000; Klinkenberg 1941):

$$\vec{V} = -\frac{k}{\mu}\left(1 + \frac{b}{p_f}\right)\nabla p_f \tag{15}$$

where k is the gas permeability, m^2. μ is the methane viscosity, Pa s. b is the Klinkenberg factor, Pa, which depends on the pore structure of the porous medium and the mean free path of the given gas molecules and generally decreases with increasing permeability(Wu and Karsten 1998). The Klinkenberg factor is given by the equation:

$$b = \alpha_k k^{-0.36} \tag{16}$$

where α_k is fitted to be 0.251, estimated from a number of experiments using 100 cores ranging in permeability from 0.01 md to 1,000 md (Jones and Owens 1980; Wu and Karsten 1998; Zhu et al. 2007; Hu et al. 2009).

By substituting Eqs. (13), (14), (15), and (16) into Eq. (12), we obtain the governing equation for the gas pressure change in the fractures:

$$\phi_f \frac{\partial p_f}{\partial t} + p_f \frac{\partial \phi_f}{\partial t} = \nabla\left(\frac{k}{\mu}\left(1 + \frac{\alpha_k k^{-0.36}}{p_f}\right) p_f \nabla p_f\right) + Q_s(1 - \phi_f) \tag{17}$$

4.3 Gas diffusion and adsorption in coal matrix

Diffusion from the coal matrix is assumed to be driven by the concentration gradient, and the gas exchange rate can be expressed as (Mora and Wattenbarger 2009; Wang et al. 2012):

$$Q_s = D\sigma_c\left(c_m - c_f\right) \tag{18}$$

where D is the gas diffusion coefficient, m^2/s. c_m is the concentration of gas in the matrix blocks, kg/m^3. c_f is the concentration of gas in the fractures, kg/m^3. σ_c is coal matrix block shape factor, m^{-2}.

According to the ideal gas law:

$$c_m = \frac{M}{\mathrm{RT}} p_m \tag{19}$$

$$c_f = \frac{M}{\mathrm{RT}} p_f \tag{20}$$

The current model incorporates the diffusion parameter using the "sorption time," which is considered to be constant for the entire production period (Mora and Wattenbarger 2009):

$$\tau = \frac{1}{\sigma_c D} \tag{21}$$

where τ is the sorption time, s. By applying the mass conservation law to the coal matrix, we obtain

$$\frac{\partial m_m}{\partial t} = -\frac{M}{\tau \mathrm{RT}}\left(p_m - p_f\right) \tag{22}$$

where m_m is the quantity of adsorbed gas and free gas per volume of coal matrix blocks, kg/m^3, which can be calculated using Langmuir equation and the ideal gas law:

$$m_m = \frac{V_L p_m}{p_m + P_L} \cdot \rho_c \cdot \rho_{gs} + \phi_m \frac{M}{\mathrm{RT}} p_m \tag{23}$$

$$\rho_{gs} = \frac{M}{V_M} \tag{24}$$

where V_L denotes the maximum adsorption capacity of coal, m^3/kg. P_L denotes the Langmuir pressure constant, MPa. ρ_c is the coal density, kg/m^3. ρ_{gs} is the gas density at standard conditions, kg/m^3. ϕ_m is the coal matrix porosity, %. V_M is the molar volume of methane under standard conditions, m^3/mol.

By substituting Eqs. (19), (20), (23), and (24) into Eq. (22), we obtain the governing equation for the gas pressure change in the coal matrix blocks:

$$\frac{\partial p_m}{\partial t} = -\frac{V_M (p_m - p_f)(p_m + P_L)^2}{\tau V_L \mathrm{RT} P_L \rho_c + \tau \phi_m V_M (p_m + P_L)^2} \tag{25}$$

4.4 Evolution of porosity and permeability

A widely used general porosity model proposed by Palmer and Mansoori (Palmer and Mansoori 1998) is used here to describe the evolution of coal fracture porosity:

$$\frac{\phi_f}{\phi_{f0}} = 1 + \frac{1}{M\phi_{f0}}[\beta_f(p_f - p_{f0}) + \beta_m(p_m - p_{m0})] + \frac{\varepsilon_L}{\phi_{f0}}\left(\frac{K}{M} - 1\right)\left(\frac{p_m}{P_L + p_m} - \frac{p_{m0}}{P_L + p_{m0}}\right) \tag{26}$$

The evolution of permeability is described by a cubic law as (Wu et al. 2010)

$$\frac{k}{k_0} = \left(\frac{\phi_f}{\phi_{f0}}\right)^3 = \left\{1 + \frac{1}{M\phi_{f0}}[\beta_f(p_f - p_{f0}) + \beta_m(p_m - p_{m0})] + \frac{\varepsilon_L}{\phi_{f0}}\left(\frac{K}{M} - 1\right)\left(\frac{p_m}{P_L + p_m} - \frac{p_{m0}}{P_L + p_{m0}}\right)\right\}^3 \tag{27}$$

where ε_L is the constant Langmuir volumetric strain at infinite pore pressure. The subscript 0 denotes the initial value of the variable. M is the constrained axial modulus, MPa, where $M = E(1-\upsilon)/[(1+\upsilon)(1-2\upsilon)]$. The change rate of porosity in fracture system can be expressed as

$$\frac{\partial \phi_f}{\partial t} = \frac{1}{M}\left(\beta_f \frac{\partial p_f}{\partial t} + \beta_m \frac{\partial p_m}{\partial t}\right) + \frac{\varepsilon_L P_L}{(P_L + p_m)^2}\left(\frac{K}{M} - 1\right)\frac{\partial p_m}{\partial t} \tag{28}$$

4.5 Coupling relationship

The pipe flow in the borehole and the methane gas migration in the coal seam are influenced by each other: The methane flow in the borehole follows the law of pipe flow, and thus, the quality of the methane from the coal seam will affect the pressure distribution along the borehole, which, in turn, will affect the former. A coupling process will thus develop due to these two types of flow (Wang et al. 2011). Coupled gas flow and solid deformation in coal seams have received considerable attention because of its importance

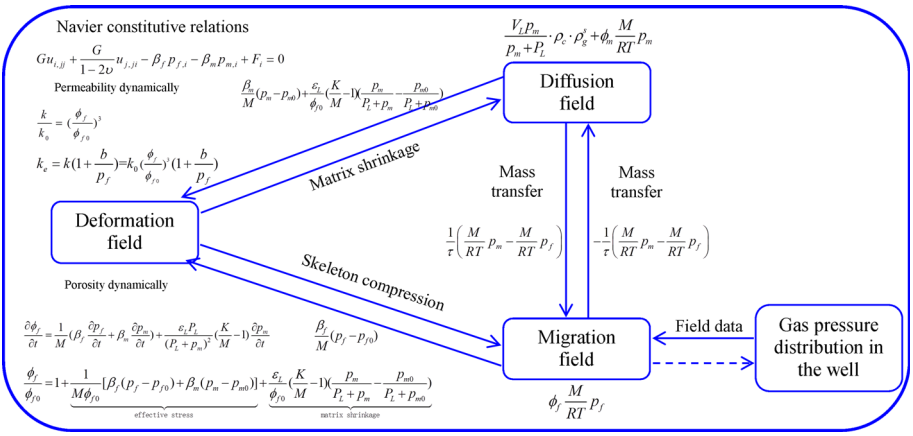

Fig. 7 Cross-couplings between pressure drop, coal deformation, gas flow in fracture system, and gas diffusion in matrix system

in such areas as pneumatic test analysis, contaminant transport, and gas outbursts during coal mining (Zhu et al. 2007; Wu and Karsten 1998; Valliappan and Zhang 1996; Zhang et al. 2008; Hu et al. 2009). The various relationships between the pressure drop in the borehole, $p(l)$; pressure in the matrix, p_m; pressure in the fractures, p_f; and permeability and dynamic porosity evolutions of the coal are plotted in Fig. 7.

While it is tempting to construct a complex, multiparameter conceptual and mathematical model to describe the interactions between pipe flow in a borehole and methane flow in coal, such a model may not lead to new insights. In particular, it is difficult to constrain and identify the parameters in complex models with sparse data sets. It is therefore difficult to establish cause-and-effect relationships with a complex model and limited data. In this study, the pressure distribution along a borehole was obtained from the field tests, and only its influence on the methane flow in coal was developed instead of the comprehensive coupling equations of pipe flow in a borehole and methane flow in coal. We believe this simplified mathematical model can capture the essential physics of these two types of flow.

5 Finite-element implementations

In the following section, we will focus on simulating the coupled gas flow in a coal seam around a methane drainage borehole, and the impact of the pressure drop on the residual gas pressure and gas content around the borehole will be discussed in detail. Then, we will obtain the effects of the pressure drop on the extraction of the coal seam gas and its further effects on mitigating the danger of coal and gas outbursts in coal seams. The numerical simulation was implemented using COMSOL Multiphysics, which provides a complete and integrated modeling environment for creating, analyzing, and visualizing multiple physical models (Multiphysics 2008).

5.1 Model description and input parameters

The geometry and boundary conditions of the simulation model are shown in Fig. 8. The settings are based on a simplification of the geometric parameters. The model's length,

width, and height are 60, 120, and 3.5 m, respectively. The radius and length of the horizontal gas drainage borehole are 48 mm and 100 m, respectively, and the sealed zone is 15 m long.

The gas flow and mechanical deformation are applied across the entire analyzed domain. In this solid deformation model, the boundary around the four sides of the model is such that the grids in the face of the model can slide in the plane but cannot move vertical to the plane. The bottom is constrained, and stress is applied to the top side. In the gas flow model, a constant pressure of 0.1 MPa is applied to the plane where the drainage borehole is drilled; all of the other five boundary surfaces are "no flow" boundaries. An initial gas pressure of 1.74 MPa is applied in the model. The input parameters used in this simulation are listed in Table 3, most of which are experimental values from the No. 21

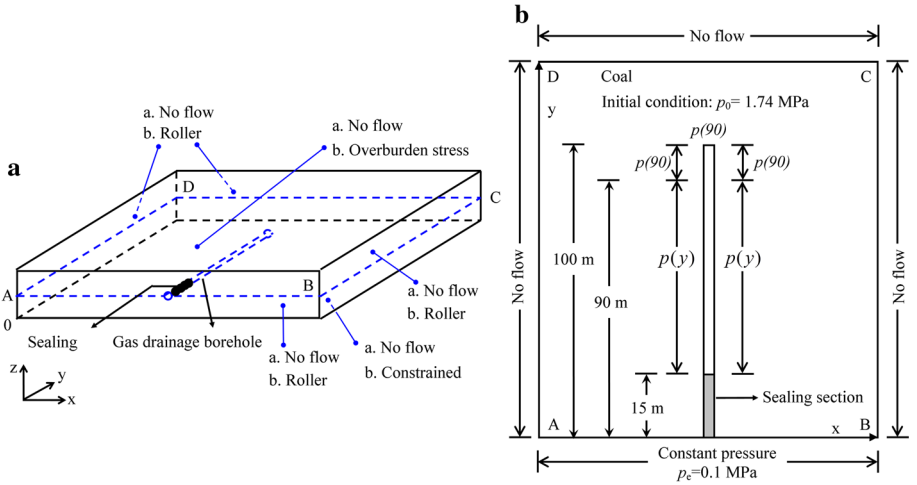

Fig. 8 Geometry and boundary conditions for the coupled mechanical deformation and gas flow process in the coal seam

Table 3 Property parameters used in the simulation model (Robertson 2005; Zhang et al. 2008)

Parameter	Value
Young's modulus of coal, E	2,713 MPa
Young's modulus of coal grains, E_m	8,143 MPa
Poisson's ratio of coal, υ	0.339
In situ stress induced by gravity, F_z	−6.5 MPa
Molar mass of methane, M	0.016 kg/mol
Temperature, T	293 K
Initial porosity of coal matrix, ϕ_{m0}	0.07
Initial porosity of fractures, ϕ_{f0}	0.012
Initial absolute gas permeability, k_0	1.38×10^{-18} m^2
Sorption time, τ	20.2 days
Langmuir pressure constant, P_L	1.3 MPa
Langmuir volume constant, V_L	0.03 m^3/kg
Langmuir volumetric strain constant, ε_L	0.02295
Density of coal, ρ_c	1,220 kg/m^3

The parameters obtained by experiments are listed in the latter part of the table

coal seam in the Jiulishan Mine, and untested parameters were taken from contemporary literature (Robertson 2005; Zhang et al. 2008).

The influence of the pressure drop on methane flow in the coal is analyzed by setting the boundary conditions of the borehole wall. The research plan and the above boundary conditions, in detail, are as follows:

Case 1: The pressure distribution applied to the boundary of the gas drainage borehole with the pressure drop is from the field tests and their fitting functions. The fitting function of the No. 12 borehole is selected. As the fitting function was developed for depths ranging from $l = 15$ m to $l = 90$ m, when $l > 90$ m, the pressures are set to equal $p(90)$.

Case 2: Case 2 involves no pressure drop in the drainage borehole; in other words, pressures along the borehole remain equal. At the same time, for the sake of comparison with Case 1, the calculated pressure $p(15)$ from the fitting function of the No. 12 borehole is applied to the boundary of the gas drainage borehole.

5.2 Gas pressure distribution around the drainage borehole

As most of the methane is stored in the coal matrix blocks, the sorption pressure is used to describe the pressure distribution around the drainage borehole. Figure 9a presents the sorption pressure distribution throughout the entire domain after having been degassed for 2 years. There are two areas with lower sorption pressures: One is in a zone directly surrounding the drainage borehole, and the other is located along the roadway wall. In Fig. 9b, the data in the various x–z planes, which start at the roadway wall, are plotted at intervals of 10 m for convenient conversion of the pressure distribution around the borehole in three-dimensional space. The minimum sorption pressure is in a zone directly surrounding the drainage borehole, and the pressure gradually increases with increasing distance from the borehole. The maximum pressure remains at the initial value of 1.74 MPa, and a single drainage borehole exhibits only limited effects. Figure 9c presents the distribution of sorption pressures along the horizontal plane $z = 1.5$ m. From this depiction, it can be clearly observed that the area around the sealed section is affected much more by the roadway wall and less by the borehole.

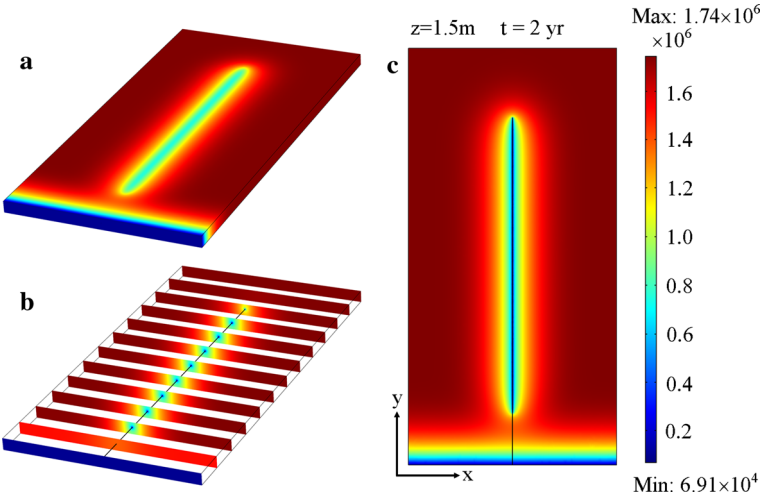

Fig. 9 Gas pressure distribution in the coal seam around a drainage borehole

Figure 10 shows the plots of the gas pressures along the horizontal lines $x = 29$ m and $x = 28$ m, both of which are in the horizontal plane $z = 1.5$ m. For the sake of contrast, the gas distribution when no pressure drop is considered and when the pressure difference is induced by the pressure drop is also plotted. The pressures along line $x = 29$ m and $x = 28$ m are divided into three segments for analysis. The length of the first segment is 15 m, which is equal to that of the sealed section, and the values along the y-axis, which corresponds to the first segment, range from 0 to 15 m. The methane in this domain corresponding to the first segment has two flow channels, namely the roadway and the drainage borehole. Due to the presence of these two flow channels, the pressure along the first segment first increases and then decreases with successive distance along the y-axis. The length of the second segment is 85 m, which is equal to that of the borehole, and the values along the y-axis corresponding to the first segment range from 15 to 100 m. The methane in this domain corresponding to the second segment is drained primarily by the borehole. Due to the influence of borehole boundary effects, the pressure at both ends of the second segment is much greater than that in the middle of the segment. At the same time, the pressure along the line $x = 29$ m is much less than that along the line $x = 28$ m in the second segment. Here, the pressure difference is used to quantify the pressure-drop effects, and this difference is obtained by subtracting the pressure calculated when the pressure drop is considered from the pressure calculated without pressure-drop effects. It can be clearly observed that the pressure difference increases with increasing displacement along the y-axis. In other words, when the effect of the pressure drop in the borehole is included, the pressure around the borehole increases with the increasing borehole depth; at the same time, the danger of coal and gas outbursts increases. The pressure difference along the line $x = 29$ m is higher than that along the line $x = 28$ m. When drainage is allowed to proceed for 2 years, the pressure differences along both lines are higher than those when drainage is allowed to proceed for 1 year. In summary, the pressure difference increases when the drainage effect is enhanced. However, it also can be observed that one can barely distinguish between the pressure distribution curves without viewing the pressure difference curves of Fig. 10. When drainage occurs over 2 years, a time that is longer than the drainage time applied in most coal mines in China, the pressure differences along lines $x = 29$ m and $x = 28$ m are lower than 4,000 and 3,000 Pa, respectively, and both of these values are lower than their corresponding residual gas pressures. The length of the third segment is 20 m, and the y-coordinate that corresponds to this third segment ranges from 100 to 120 m. There is small decline in the methane pressure in this area corresponding to the third segment, as it is affected only by the end of the borehole.

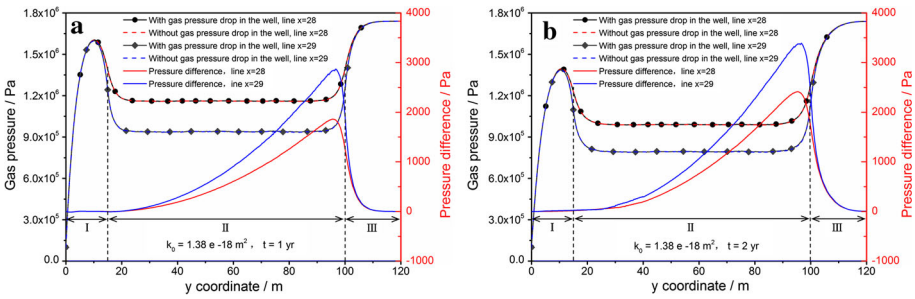

Fig. 10 Gas pressure distribution along the horizontal lines $x = 28$ m and $x = 29$ m

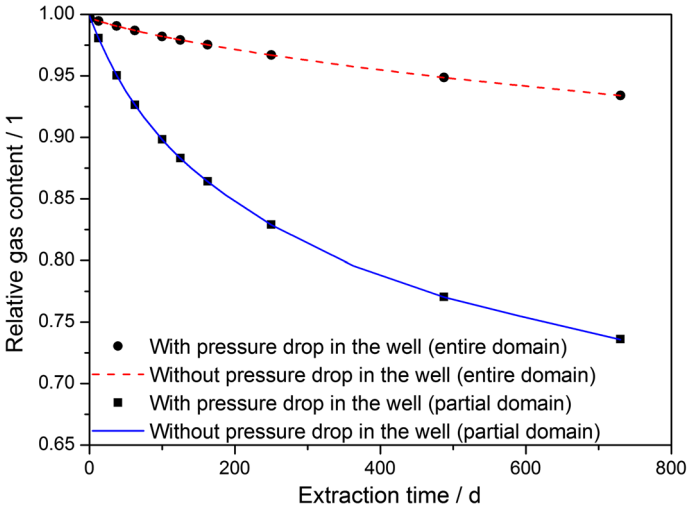

Fig. 11 The relative gas content in the coal seam at various times (the relative gas content is obtained when the gas mass at a time is divided by the initial gas mass)

5.3 Gas content evolution

In this numerical simulation, the gas stored in the coal seam is drained gradually, and the degasification speed reduces gradually, as shown in Fig. 11. For the entire calculational domain, after a drainage period of 2 years, the relative gas content is still higher than 93 %, which is achieved by the roadway wall and drainage borehole acting together. Due to the low permeability of the No. 21 coal seam in the Jiulishan Mine, a single borehole clearly has only a limited effect on the degassing of the coal seam. At the same time, one can barely distinguish the difference between the two relative gas content curves. Because the effects of the pressure drop accumulate when the drainage effect is enhanced, as we concluded in the previous section, we then calculated the relative gas content of a smaller domain. This new domain was obtained in two cross sections of the original domain, namely the y–z planes $x = 28$ m and $x = 32$ m. For the new calculational domain (partial calculation domain), after a drainage period of 2 years, the relative gas content declined to approximately 75 %, and thus, drainage engineering to increase the number of boreholes will help in degassing the coal more rapidly. However, we are still barely able to distinguish any difference between the two relative gas content curves.

6 Conclusions

In this study, the differences between the causes of pressure drops in horizontal wells and in drainage boreholes were researched. We concluded that the conventional pressure-drop models may not be useful in developing predictions of the pressure drops in a drainage borehole in a coal seam. Given this background, 18 sets of field tests were performed to develop an understanding of the distribution of pressure drops along a drainage borehole in a coal seam. The experimental results indicate that the pressures ranged from 58.7 to 76.1 kPa at the outer ends of the boreholes and from 66.4 to 80.4 kPa at a depth of 90 m in the boreholes. The pressure increased in a parabolic form with increasing depth in the

borehole. In addition, the lower the pressure at the outer end, the larger the pressure gradient in a borehole. A fitting function was obtained and used to calculate the pressures at various locations in a borehole, and this function displays good fitting precision.

To obtain the quantitative effects of the pressure drop on the extraction of gas from the coal seam and its further effects on mitigating the danger of coal and gas outbursts in the Jiulishan Mine, a coupled finite-element model, which includes the pressure drop in the borehole, Darcy flow in the fractures, gas diffusion in the matrix blocks, and dynamic evolution of the permeability of the coal seam, was developed. In particular, the effects of the pressure drop of methane flow in the coal were analyzed by setting certain boundary conditions of the borehole wall. All of the governing equations were implemented in COMSOL Multiphysics, which provides a complete and integrated modeling environment for creating, analyzing, and visualizing multiphysics models. The numerical results indicate that due to the pressure drop in the drainage borehole, the pressure around the borehole increases with the increase in the borehole depth and the pressure gradient increases with the enhanced drainage effect of the borehole. However, after a drainage period of 2 years, a time period that is longer than the drainage time applied in most coal mines in China, the pressure gradient is far lower than the residual gas pressure. At the same time, the difference in the relative gas content induced by pressure drop is very small. In summary, the pressure drop does affect the coal seam gas extraction, but the impact is very small and can be ignored in engineering.

In the future, the operators of the Jiulishan Mine should pay greater attention to drainage borehole design and construction quality and need not give undue consideration to the effects of pressure drops in drainage boreholes.

Acknowledgments This work was supported by the Natural Science Foundation for the Youth of China (No. 41202118, No. 51204173), the National Basic Research Program of China (973 Program, No. 2011CB201204), and the Natural Science Foundation for the Youth of China (No. 51304204).

References

Amna G, Hiroshi T (2011) Experimental study and modeling of pressure loss for foam-cuttings mixture flow in horizontal pipe. J Hydrodyn Ser B 23(4):431–438

Awwad A, Xin R, Dong Z, Ebadian M, Soliman H (1995) Measurement and correlation of the pressure drop in air-water two-phase flow in horizontal helicoidal pipes. Int J Multiph Flow 21(4):607–619

Badie S, Hale C, Lawrence C, Hewitt G (2000) Pressure gradient and holdup in horizontal two-phase gas–liquid flows with low liquid loading. Int J Multiph Flow 26(9):1525–1543

Dikken B (1990) Pressure drop in horizontal wells and its effect on production performance. J Petrol Technol 42(11):1426–1433

Firoozabadi HM, Rahimzade K, Pourafshari P (2011) Field validation of pressure drop models in perforated section of gas condensate wells. J Nat Gas Sci Eng 3(2):375–381

Gilman A, Beckie R (2000) Flow of coal-bed methane to a gallery. Transp Porous Media 41(1):1–16

Gong X, Tian J, Wang J (2013) First integral method for an oscillator system. Electron J Differ Equ 96:1–12

Guo B (2010) Corrections to horizontal drain hole productivity equations for wellbore friction effect. J Petrol Sci Eng 70(3):344–349

Hu G, Wang H, Fan X, Yuan Z, Hong S (2009) Mathematical model of coalbed gas flow with Klinkenberg effects in multi-physical fields and its analytic solution. Transp Porous Media 76(3):407–420

Jin R, Chen W, Simpson TW (2001) Comparative studies of metamodelling techniques under multiple modelling criteria. Struct Multidiscip Optim 23(1):1–13

Jones FO, Owens W (1980) A laboratory study of low-permeability gas sands. J Petrol Technol 32(9):1631–1640

Klinkenberg L (1941) The permeability of porous media to liquids and gases. In: Drilling and production practice. American Petroleum Institute, New York, pp 200–213

Li GZ, Yao YD, Dong SP (2007) A physical model for predicting the pressure drop of gas-liquid slug flow in horizontal pipes. J Hydrodyn 19(6):736–742. doi:10.1016/s1001-6058(08)60011-6
Mian C, Zhida C (1999) Effective stress laws for multi-porosity media. Appl Math Mech 20(11):1207–1213
Mora C, Wattenbarger R (2009) Analysis and verification of dual porosity and CBM shape factors. J Can Pet Technol 48(2):17–21
Multiphysics C (2008) User's guide, version 3.5 a. COMSOL AB
Novy R (1995) Pressure drops in horizontal wells: when can they be ignored? SPE Reserv Eng 10(1):29–35
Olivier JG, Van Aardenne JA, Dentener FJ, Pagliari V, Ganzeveld LN, Peters JA (2005) Recent trends in global greenhouse gas emissions: regional trends 1970–2000 and spatial distribution of key sources in 2000. Environ Sci 2(2–3):81–99
Ouyang L-B, Aziz K (2000) A homogeneous model for gas–liquid flow in horizontal wells. J Petrol Sci Eng 27(3):119–128
Pabst W, Gregorová E, Tichá G (2006) Elasticity of porous ceramics—A critical study of modulus–porosity relations. J Eur Ceram Soc 26(7):1085–1097
Palmer I, Mansoori J (1998) How permeability depends on stress and pore pressure in coalbeds: a new model. SPE Reservoir Eval Eng 1(6):539–544
Qu P, Shen R, Fu L, Wang Z (2011) Time delay effect due to pore pressure changes and existence of cleats on borehole stability in coal seam. Int J Coal Geol 85(2):212–218. doi:10.1016/j.coal.2010.10.013
Robertson E (2005) Modeling permeability in coal using sorption-induced strain data. In: SPE annual technical conference and exhibition
Sarica C, Haciislamoglu M, Raghavan R, Brill J (1994) Influence of wellbore hydraulics on pressure behavior and productivity of horizontal gas wells. In: SPE annual technical conference and exhibition
Shen B, Liu J, Zhang H (2007) The technical measures of gas control in China coal mines [J]. J China Coal Soc 7:000
Su Z, Gudmundsson J (1998) Perforation inflow reduces frictional pressure loss in horizontal wellbores. J Petrol Sci Eng 19(3):223–232
Valliappan S, Zhang W (1996) Numerical modelling of methane gas migration in dry coal seams. Int J Numer Anal Meth Geomech 20(8):571–593
Wang Z-M, Xiao J-N, Wang X-Q, Wei J-G (2011) Experimental study for pressure drop of variable mass flow in horizontal well. Shiyan Liuti Lixue/J Exp Fluid Mech 25(5):26–29
Wang J, Kabir A, Liu J, Chen Z (2012) Effects of non-Darcy flow on the performance of coal seam gas wells. Int J Coal Geol 93:62–74
Wu Y-S, Karsten P (1998) Gas flow in porous media with Klinkenberg effects. Transp Porous Media 32(1):117–137
Wu Y, Liu J, Elsworth D, Chen Z, Connell L, Pan Z (2010) Dual poroelastic response of a coal seam to CO_2 injection. Int J Greenhouse Gas Control 4(4):668–678
Yao X, Cheng G, Shi B (2010) Analysis on gas extraction drilling instability and control method of pore-forming in deep surrounding-rock with weak structure. J China Coal Soc 35(12):2073–2081
Yu L-X, Zhou S-T, Zhang Q (2001) Pressure gradient model for variable mass fluid flow in horizontal wellbore. Shiyou Daxue Xuebao/J Univ Petroleum China 25(4):47–48
Yuan H, Sarica C, Brill J (1996) Effect of perforation density on single phase liquid flow behavior in horizontal wells. In: International conference on horizontal well technology
Zhang J, Roegiers J-C, Bai M (2004) Dual-porosity elastoplastic analyses of non-isothermal one-dimensional consolidation. Geotech Geol Eng 22(4):589–610
Zhang H, Liu J, Elsworth D (2008) How sorption-induced matrix deformation affects gas flow in coal seams: a new FE model. Int J Rock Mech Min Sci 45(8):1226–1236
Zhu W, Liu J, Sheng J, Elsworth D (2007) Analysis of coupled gas flow and deformation process with desorption and Klinkenberg effects in coal seams. Int J Rock Mech Min Sci 44(7):971–980